Mathematics and Systems Science 2025, 3(2), 2991.
https://doi.org/10.54517/mss2991

Asia Pacific Academy of Science Pte. Ltd.

Article

Effects of solar sail and various perturbations under the equilateral triangular configuration in the four interacting bodies problem

Abdullah

Department of Mathematics, Dyal Singh College, University of Delhi, Delhi 110003, India; abdullah.maths@dsc.du.ac.in

CITATION

Abdullah. Effects of solar sail and various perturbations under the equilateral triangular configuration in the four interacting bodies problem. Mathematics and Systems Science. 2025; 3(2): 2991. https://doi.org/10.54517/mss2991

ARTICLE INFO

Received: 8 August 2024
Accepted: 26 February 2025
Available online: 2 April 2025

Abstract: Solar sail and other perturbation effects are studied on the dynamical motion of the infinitesimal body in the four interacting bodies where three bigger bodies (two out of these three bodies are oblate in shape and equal in size) are situated at the vertices of an equilateral triangle. The important dynamical properties, like the locations of equilibrium points, their stability, the periodic orbits, Poincaré surfaces of section, and the basins of attraction, are illustrated with the evaluated equations of motion in unperturbed and perturbed cases. This investigation will be helpful to the space agencies worldwide.

Keywords: solar sail; oblateness; interactions; asteroids belts; equilateral triangular configuration

MSC: 70F05; 70F15; 37N05

1. Introduction

A device where the energy stored which is generated from sunlight through a large surfaces is known as a solar sail or light sail. Many spacecraft missions have been introduced for solar propulsion and navigation. Due to solar sail craft occurs low-cost operations combined with long operating lifetimes. As it has some moving parts, it can effectively be used many times for the delivery of payloads.

Radiation pressure affects all spacecraft during the interplanetary space mission or during motions. Whenever the spacecraft is going towards a planet, it will be displaced by solar radiation pressure to thousands of kilometers, therefore the effects must be taken into account at the time of trajectory planning. A new factor must be added in spacecraft design because solar pressure affects the orientation of a spacecraft.

In the existing literature, we found that many scientists and researchers have studied the effects of solar sails with the different aspects of the circular restricted 3-body problem. These perturbations played an important role in the motion properties. Some of these researchers have investigated as:

The dynamical motions of the geocentric orbiting high-performance solar sail in the co-rotating reference frame where the axis is directed along the primary bodies are analyzed in [1, 2]. The mathematical structure for describing the acceleration experienced by a solar sail are investigated in [3–8]. The dynamics of a solar sail by supposing the radiated Earth-Sun restricted 3-body problem is modeled in [9,10]. They also have computed the center manifold around different equilibria. The design of a solar-sail spacecraft in two sequential steps are explored in [11, 12]. A shape-based approach for solar sailing has been developed. The authors have investigated the dynamical properties of the motion of the infinitesimal body in the restricted three-body

problem by assuming the interaction between the primary bodies in [13–15]. The restricted 3-body problem by assuming the effects of solar sails are investigated in [16]. The effects of asteroid belts on the motion properties in the restricted problem are investigated in [17–26]. The motion properties under the effects of variable mass and other perturbations in the restricted problems are revealed in [27–35].

With the influence of the above literatures, in the present paper, we have considered the effect of solar sails on the motion with some other perturbations in the restricted 4-body problem. Where two out of these bigger bodies are oblate in shape as well as equal in size. Also these bodies are interacting with each other and surrounded by the asteroid belts.

This paper is organized in various sections. The brief introduction of the literature is given in Section 1. The presentation of the problem is performed in Section 2. Section 3 illustrates the investigations numerically for the problem with various subsections. The paper concludes in Section 4.

2. Presentation of the problem

In this four-body configuration, we suppose that three bigger bodies of masses m_1, m_2 and m_3 (where m_2 and m_3 are equal and oblate in shape with oblateness parameters A_2 and A_3 respectively) are placed at the vertices of an equilateral triangle of side ℓ. The primary bodies are revolving around their common center of mass in circular orbits with the mean motion ν. While the fourth body of mass m is moving in space under the gravitational effects of the three bigger bodies including their interaction with the interaction parameter K, the asteroids-belt with mass parameter M_b and the solar sail effects with the sail components S_x, S_y and S_z in the x, y and z directions respectively and the Coriolis as well as centrifugal forces with parameters δ_1 and δ_2 respectively. The overview of the configuration of the problem can be found in **Figure 1**. Following the procedures given by [36–40], the equations of motion of the infinitesimal body can be written as:

$$\begin{aligned} -2\,\delta_1\,\nu\,\dot{y} + \ddot{x} &= \mathbf{\Pi}_x + S_x, \\ 2\,\delta_1\,\nu\,\dot{x} + \ddot{y} &= \mathbf{\Pi}_y + S_y, \\ \ddot{z} &= \mathbf{\Pi}_z + S_z, \end{aligned} \tag{1}$$

with

$$\mathbf{\Pi} = \frac{\delta_2\,\nu^2}{2}(x^2+y^2)+\frac{1-2\mu}{r_1}+\frac{\mu}{r_2}+\frac{\mu}{r_3}+\frac{\mu\,A_2}{2\,r_2^3}+\frac{\mu\,A_3}{2\,r_3^3}+\frac{K}{r_1\,r_2\,r_3}+\frac{M_b}{(r^2+T^2)^{1/2}},$$

$$S_x = S\left[\frac{x-\sqrt{3}\,\mu}{r_1}\,Cos\,\alpha-\frac{(x-\sqrt{3}\,\mu)\,z}{r_1\,r_s}\,Sin\,\alpha\cdot Cos\,\psi+\frac{y}{r_s}\,Sin\,\alpha\cdot Sin\,\psi\right],$$

$$S_y = S\left[\frac{y}{r_1}\,Cos\,\alpha-\frac{y\,z}{r_1\,r_s}\,Sin\,\alpha\cdot Cos\,\psi-\frac{x-\sqrt{3}\,\mu}{r_s}\,Sin\,\alpha\cdot Sin\,\psi\right],$$

$$S_z = S\left[\frac{z}{r_1}\,Cos\,\alpha+\frac{r_s}{r_1}\,Sin\,\alpha\cdot Cos\,\psi\right],\quad S=\frac{q_0\,(1-2\,\mu)}{r_1^2}\cdot Cos^2\,\alpha,$$

$$r^2 = x^2+y^2+z^2,\ r_s^2=(x-\sqrt{3}\,\mu)^2+y^2,\ r_1^2=(x-\sqrt{3}\,\mu)^2+y^2+z^2,$$

$$r_2^2 = (\tfrac{\sqrt{3}}{2}(1-2\mu)+x)^2+(y-\tfrac{1}{2})^2+z^2,\quad r_3^2=(\tfrac{\sqrt{3}}{2}(1-2\mu)+x)^2+(y+\tfrac{1}{2})^2+z^2,$$

$$\mu = \frac{m_2}{m_1+m_2+m_3},\ \nu^2=1+K+\frac{3}{2}(A_2+A_3)+\frac{2\,M_b\,r_c}{(r_c^2+T_0^2)^{3/2}},\ r_c=3\,\mu,$$

T = $a+\sqrt{z^2+b^2}$, $T_0=a+b$, $a\,\&\,b$ = flatness parameter & core parameter of the belt respectively,

α = orientation of the solar panel $\in[-\pi/2,\ \pi/2]$, q_0 = the radiation parameter,

ψ = clock angle $\in[0,\ \pi]$, δ_1 & δ_2 = coriolis and centrifugal forces parameters respectively,

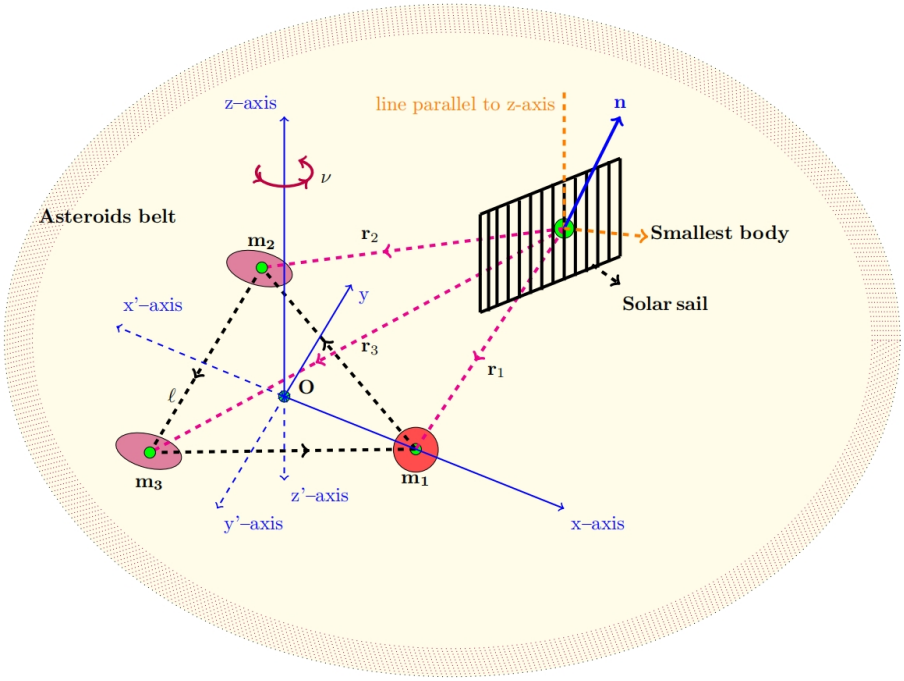

Figure 1. Interactions in the perturbed restricted 4-body equilateral triangular configuration with solar sail.

The indices x, y, z in suffixes with Π are denoting the partial derivatives with respect to these indices. If we ignore the perturbations taken here then this problem will become a classical restricted four-body problem where the mean motion will be unity.

3. Numerical investigations

The most important dynamical properties, i.e., positions of equilibrium points, their stability, periodic orbits, PSS and basins of attractions are illustrated in unperturbed and perturbed cases with the use of Mathematica software.

3.1. Equilibrium points

We have determined the locations of equilibrium points of in-plane motion (i.e., in x-y plane) from Equation (1) by solving

$$\begin{aligned} \mathbf{\Pi}_x &+ S_x = 0, \\ \mathbf{\Pi}_y &+ S_y = 0, \end{aligned} \tag{2}$$

with the numerical values as $z = 0$, $\mu = 0.2$, $\delta_1 = \delta_2 = 1.2$, $\theta = \pi/4$, $\phi = \pi/4$, $q = 0.2$, $A_2 = 0.001$, $A_3 = 0.00015$, $M_b = 0.2$, $T_0 = 0.2$ and $K = 0.4$.

The equilibrium points of in-plane motion are performed in the two cases (perturbed and unperturbed cases). In both cases eight equilibrium points exist, where in the unperturbed case (**Figure 2a**) two collinear equilibrium points ($L_{1,2}$) and six non-collinear equilibrium points ($L_{3,4,5,6,7,8}$) exist, while in the perturbed case (**Figure 2b**) only one collinear equilibrium point (L_1) and seven non-collinear equilibrium points ($L_{2,3,4,5,6,7,8}$) exist. In both cases, the non-collinear equilibrium points L_3 and L_4, L_5 and L_6, L_7 and L_8 are symmetrical about the x-axis. We also observed that with perturbations, the positions of equilibrium points are shrinking towards the origin.

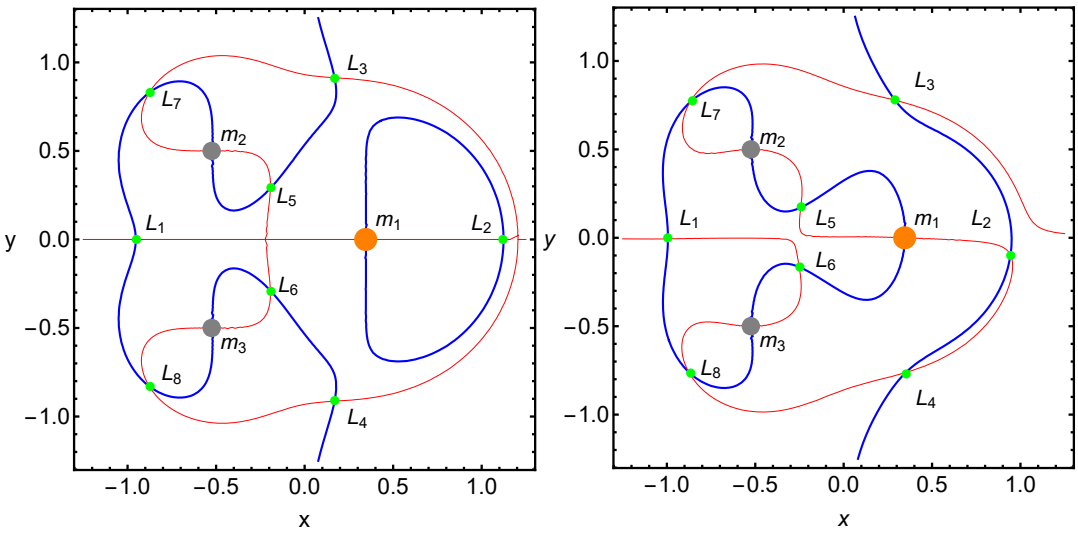

(a) Unperturbed case. **(b)** Perturbed case.

Figure 2. The gray and orange color dots are representing the locations of primary bodies while green color dots are representing the locations of equilibrium points.

3.2. Stability states

The equations of motion i.e. Equation (1) can be written as

$$\begin{aligned} -2\,\delta_1\,\nu\,\dot{y} + \ddot{x} &= P_x \\ 2\,\delta_1\,\nu\,\dot{x} + \ddot{y} &= P_y \\ \ddot{z} &= P_z \end{aligned} \tag{3}$$

where, $P_x = \mathbf{\Pi}_x + S_x$, $P_y = \mathbf{\Pi}_y + S_y$ and $P_z = \mathbf{\Pi}_z + S_z$.

By shifting the equilibrium point $(x_0,\, y_0,\, z_0)$ to the point $(\xi,\, \eta,\, \zeta)$ in Equation (3), one can examine the stability, hence

$$\begin{aligned} \ddot{\xi} - 2\,\delta_1\,\nu\,\dot{\eta} &= P^0_{x\,x}\,\xi + P^0_{x\,y}\,\eta + P^0_{x\,z}\,\zeta, \\ \ddot{\eta} + 2\,\delta_1\,\nu\,\dot{\xi} &= P^0_{y\,x}\,\xi + P^0_{y\,y}\,\eta + P^0_{y\,z}\,\zeta, \\ \ddot{\zeta} &= P^0_{z\,x}\,\xi + P^0_{z\,y}\,\eta + P^0_{z\,z}\,\zeta. \end{aligned} \tag{4}$$

If $\xi = A\,e^{\lambda\,t}$, $\eta = B\,e^{\lambda\,t}$ and $\zeta = C\,e^{\lambda\,t}$ are the solutions of the Equation (4), then this equation gives as

$$\begin{aligned} A\,(\lambda^2 - P^0_{x\,x}) \quad & -B\,(2\,\delta_1\,\nu + P^0_{x\,y}) \quad -C\,P_{x\,z} \quad = \quad 0, \\ A\,(2\,\delta_1\,\nu\,\lambda - P^0_{y\,x}) \quad & +B\,(\lambda^2 - P^0_{y\,y}) \quad -C\,P^0_{y\,z} \quad = \quad 0, \\ -A\,P^0_{z\,x} \quad & -B\,P^0_{z\,y} \quad +C\,(\lambda^2 - P^0_{z\,z}) \quad = \quad 0, \end{aligned} \tag{5}$$

The trivial solution can be obtained if

$$\begin{vmatrix} (\lambda^2 - P^0_{x\,x}) & -(2\,\delta_1\,\nu + P^0_{x\,y}) & -P_{x\,z} \\ (2\,\delta_1\,\nu\,\lambda - P^0_{y\,x}) & (\lambda^2 - P^0_{y\,y}) & -P^0_{y\,z} \\ -P^0_{z\,x} & -P^0_{z\,y} & +(\lambda^2 - P^0_{z\,z}) \end{vmatrix} = 0 \tag{6}$$

And hence the characteristic equation corresponding to Equation (6) will be:

$$\lambda^6 + P_4\,\lambda^4 + P_3\,\lambda^3 + P_2\,\lambda^2 + P_1\,\lambda + P_0 = 0, \tag{7}$$

where,

$$P_4 = -(P^0_{x\,x} + P^0_{y\,y} + P^0_{z\,z}),$$

$$P_3 = 2\,\delta_1\,\nu\,(P^0_{x\,y} + 2\,\delta_1\,\nu),$$

$$\begin{aligned} P_2 = {} & P^0_{x\,x}\,P^0_{y\,y} + P^0_{x\,x}\,P^0_{z\,z} + P^0_{y\,y}\,P^0_{z\,z} - (P^0_{x\,y})^2 \\ & - (P^0_{x\,z})^2 - (P^0_{y\,z})^2 - 2\,P^0_{x\,y}\,\delta_1\,\nu, \end{aligned} \tag{8}$$

$$P_1 = 2\,\delta_1\,\nu\,(P^0_{x\,z}\,P^0_{y\,z} - P^0_{x\,y}\,P^0_{z\,z} - 2\,P^0_{z\,z}\,\delta_1\,\nu),$$

$$\begin{aligned} P_0 = {} & (P^0_{x\,z})^2\,P^0_{y\,y} + P^0_{x\,x}\,(P^0_{y\,z})^2 + (P^0_{x\,y})^2\,P^0_{z\,z} - P^0_{x\,x}\,P^0_{y\,y}\,P^0_{z\,z} \\ & - 2\,P^0_{x\,y}\,P^0_{x\,z}\,P^0_{y\,z} - 2\,P^0_{x\,z}\,P^0_{y\,z}\,\delta_1\,\nu + 2\,P^0_{x\,y}\,P^0_{z\,z}\,\delta_1\,\nu. \end{aligned}$$

We numerically solved the Equation (6) corresponding to each equilibrium point and given in **Tables 1** and **2**. From where, we observed that at least one root is either a positive real value or a positive real part of the complex roots. Hence, the instability of these equilibrium points.

Table 1. Nature in the unperturbed case.

Equilibrium points	***Roots***	***Nature***
L_1	Positive real part of a complex root	*Unstable*
L_2	Positive real value	*Unstable*
$L_{3,4}$	Positive real part of a complex root	*Unstable*
$L_{5,6}$	Positive real value	*Unstable*
$L_{7,8}$	Positive real value	*Unstable*

Table 2. Nature in the perturbed case-III.

Equilibrium points	***Roots***	***Nature***
L_1	Positive real part	*Unstable*
L_2	Positive real value	*Unstable*
$L_{3,4}$	Positive real part	*Unstable*
$L_{5,6}$	Positive real value	*Unstable*
$L_{7,8}$	Positive real value	*Unstable*

3.3. Periodic orbits

With the proper choice of the initial values, we have to solve the equations of motion by rewriting them in the phase space and then with the use of well-known software Mathematica, we have drawn the periodic orbits in two cases (the unperturbed case and the perturbed case). **Figure 3a** represents the periodic orbits in the unperturbed case. In this case, the initial values are $x[0] = 0.000000005$, $y[0] = -0.01$, $\dot{x}[0] = 0.000000005$, $\dot{y}[0] = 0$, for which the time period is 19.1 units. But in the perturbed case, the initial values are $x[0] = 0.345$, $y[0] = 0$, $\dot{x}[0] = 0.345$, $\dot{y}[0] = 0$, for which the

time period is 16.73 units. In both cases, the orbits are not simply periodic. Further in the unperturbed case, the motion covers more time and less area in comparison to the perturbed case. We also observed from both cases that in the unperturbed case, the initial values are smaller and the time period is greater than in the perturbed case.

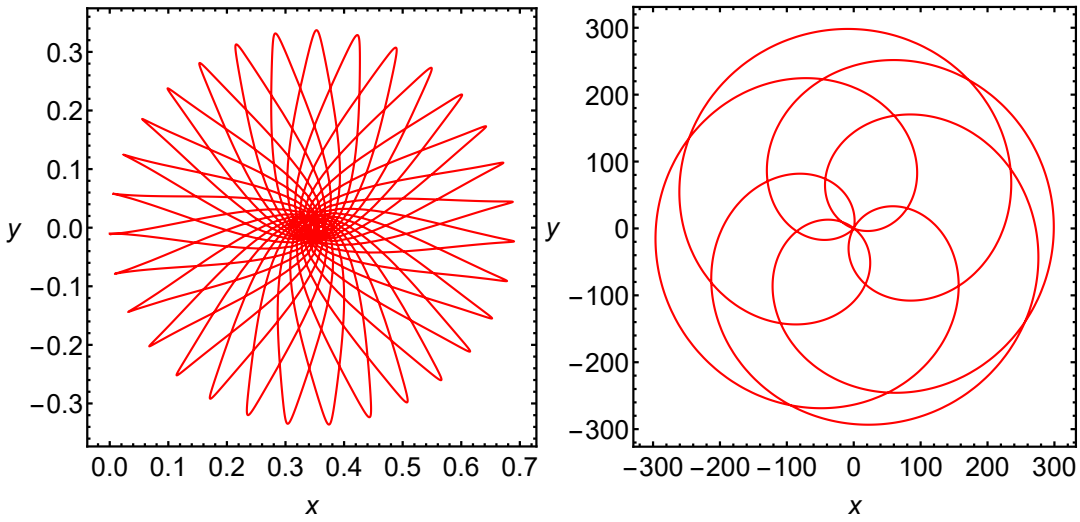

(a) Unperturbed case. **(b)** Perturbed case.

Figure 3. Periodic orbits.

3.4. Poincaré surfaces of section (PSS)

Chaotic and non-chaotic regions explain the important dynamical behavior of the motion, therefore we have plotted the PSS for both cases (the unperturbed case and the perturbed case). For this, we have to evaluate the location (x, y) and velocity $(\dot{x}, \dot{y})$ of the infinitesimal body and then draw the graph between $(x, \dot{x})$ at $y = 0$, whenever the path intersects the plane for $\dot{y} > 0$. **Figure 4a**,**b** represents the unperturbed case and perturbed case respectively. We observed in both cases there is no chaos and surfaces are symmetrical about both the axes. There is no chaos means the motion will be regular and symmetrical means that if we study the behavior of the motion in the first quadrant or just one part of the four parts of the figure then we can similarly say the behavior of the other three parts of the figure.

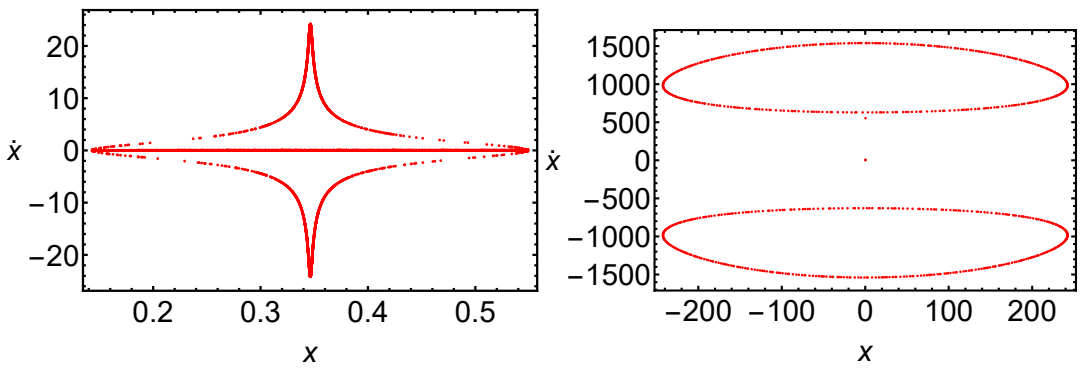

(a) Unperturbed case. **(b)** Perturbed case.

Figure 4. Poincaré surfaces of section.

3.5. Basins of attraction

For the basins of attraction, we will follow the procedure given by [41] where they have used the Newton's-Raphson iterative method. This method is easier, faster and simpler than the other methods. The iterative algorithm for our problem is as follows:

$$\begin{cases} x_{n+1} = x_n - \left(\dfrac{P_x P_{yy} - P_y P_{xy}}{P_{xx} P_{yy} - P_{xy} P_{yx}} \right)_{(x_n\, y_n)}, \\ y_{n+1} = y_n - \left(\dfrac{P_y P_{xx} - P_x P_{yx}}{P_{xx} P_{yy} - P_{xy} P_{yx}} \right)_{(x_n\, x_n)}, \end{cases} \tag{9}$$

where the n-th step of the Newton-Raphson iterative method for x and y can be taken as x_n, y_n, and also the denominators must be non-zero in Equation (9).

If all the points are converge to one of the attracting points (equilibrium points) then the basins of the attracting domain are generated. The color code will be used to differentiate the attracting regions. The basins of attraction are performed in two cases (unperturbed case and perturbed case) and presented in **Figure 5** with two **Figure 5a**,**b**. **Figure 5a**,**b** represents the basins of attraction for the unperturbed case and the perturbed case respectively. For the clear view, the number of iterations is taken as 28 and 22 for the unperturbed case and perturbed case respectively. We observed that the number of iterations is reduced due to perturbations.

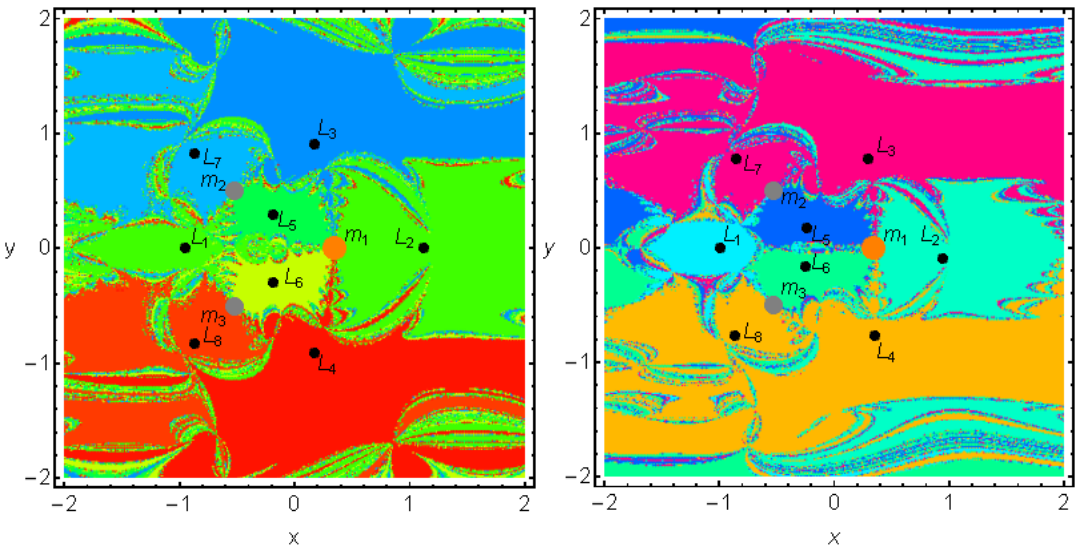

(a) Unperturbed case. **(b)** Perturbed case.

Figure 5. Basins of attraction.

From **Figure 5a**, we observed that the attracting points $L_{1,\,2,\,5}$ correspond to the green color regions, the attracting points $L_{3,\,7}$ correspond to the light blue color regions, the attracting point L_6 corresponds to the yellow color region, the attracting points $L_{4,\,8}$ correspond to the red color region. And these regions corresponding to the attracting points are extended to infinity except the region corresponding to the attracting point L_6.

From **Figure 5b**, we observed that the attracting point L_1 corresponds to the cyan

color region, the attracting point L_2 corresponds to the light green color region, the attracting points $L_{3,7}$ correspond to the dark pink color regions, the attracting points L_5 and L_6 correspond to the blue and green color regions respectively, the attracting points $L_{4,8}$ correspond to the dark yellow color regions. In this way, the regions corresponding to the attracting points $L_{1,5,6}$ are finite and the rest of the regions are extended to infinity. We also observed from here that due to perturbations the color codes and the number of iterations were changed in comparison to the unperturbed case.

4. Conclusion

The impact of the solar sail including other perturbations (like interaction between bodies, asteroid belts, oblateness, etc.) is investigated on the motion of the infinitesimal body in the circular restricted 4-body problem. Firstly, the analytical determination of the equation of motion shows these impacts. And then numerically, we have illustrated the dynamical properties in two cases (unperturbed and perturbed cases). From where we have observed that the number of collinear equilibriums is reducing and the positions of the equilibrium points are shrinking towards the origin in the perturbed case than the unperturbed case. And found that all the equilibrium points are unstable in both cases.

With the use of the initial values, we got the periodic orbits in both cases but these periodic orbits are multiply periodic with different time periods. In the next, we have obtained the Poincaré surfaces of sections that are symmetrical about both the axes and there is no chaos. Further, the basins of attractions are illustrated in both cases, where we have used the color code to bifurcate the attracting regions. We found here that most of the attracting regions are extended to infinity. In this way, these properties clearly show the impact of the perturbations.

If an infinitesimal body is moving in space with these perturbations, then one can get the location of equilibrium points nearer than without perturbations. Means space stations can be installed with lower prices because distances are also a big factor.

We also found that due to perturbations, the time periods are less than due to the un-perturbations, meaning an infinitesimal body can reach faster with perturbations than the un-perturbations to the destination.

Acknowledgments: We are thankful to the International center for advanced interdisciplinary research (ICAIR), New Delhi, India for providing the research facilities.

Institutional review board statement: Not applicable.

Informed consent statement: Not applicable.

Conflict of interest: The author declares no conflict of interest.

References

1. McInnes CR, Simmons JFL. Solar sail halo orbits I: Heliocentric case. J. Spacecr. Rockets. 1992; 29(4): 466–471.
2. McInnes CR, Simmons JFL. Solar sail halo orbits II: Geocentric case. J. Spacecr. Rockets. 1992; 29(4): 472–479.
3. McInnes CR, McDonald AJC, Simmons JFL, MacDonald EW. Solar sail parking in restricted three-body system. J. Guid. Control Dyn. 1994; 17(2): 399–406.

4. McInnes A. Strategies for Solar Sail Mission Design in the Circular Restricted Three-Body Problem [Master's thesis]. Purdue University; 2000.
5. McInnes CR, MacDonald M, Angelopolous V, Alexander D. GEOSAIL: Exploring the geomagnetic tail using a small solar sail. J. Spacecr. Rockets. 2001; 38(4): 622–629.
6. Macdonald M, Hughes G, McInnes C, et al. Geo-sail: An elegant solar sail demonstration mission. J. Spacecr. Rockets. 2007; 44(6): 784–796.
7. Mengali G, Quarta A, Circi C, Dachwald B. Refined solar sail force model with mission application. J. Guid. Control Dyn. 2007; 30(2): 512–520
8. Heiligers J, Mingotti G, McInnes CR. Optimal solar sail transfers between halo orbits of different sun-planet systems. Adv. Space Res. 2015; 55: 1405–1421.
9. Farrés A. Contribution to the Dynamics of a Solar Sail in the Earth-Sun System [PhD thesis]. Universitat de Barcelona; 2009.
10. Farrés A, Jorba A. Periodic and quasi-periodic motions of a solar sail around the family SL_1 on the Sun-Earth system. Celest. Mech. Dyn. Astron. 2010; 107: 233–253.
11. Gong S, Li J. Solar sail heliocentric elliptic displaced orbits. J. Guid. Control. Dyn. 2014; 37(64): 2021–2025.
12. Peloni A, Ceriotti M, Dachwald B. Solar-sail trajectory design for a multiple near-Earth-asteroid rendezvous mission. J. Guid. Control Dyn. 2016; 39: 2712–2724.
13. Bosanac N, Howell K, Fischbach E. A natural autonomous force added in the restricted problem and explored via stability analysis and discrete variational mechanics. Astrophys. Space Sci. 2016; 361: 49.
14. Ragos O, Perdiou A, Perdios E. The three-body interaction effect on the families of 3D periodic orbits associated to sitnikov motion in the circular restricted three-body problem. The Journal of the Astronautical Sciences. 2020; 67: 28–58.
15. Ragos O. Short and long period periodic orbits around a stable collinear equilibrium point in the circular restricted three-body problem with a three-body interaction. New Astron. 2022; 98(1): 101900.
16. Sood R, Howell K. Solar Sail transfers and trajectory design to Sun-Earth L_4, L_5; Solar observations and potential Earth Trojan Exploration. The Journal of the Astronautical Sciences. 2019.
17. Miyamoto M, Nagai R. Three-dimensional models for the distributation of mass in Galaxies. Publ. Astron. Soc. Japan. 1975; 27: 533–543.
18. Singh J, Taura JJ. Motion in the generalized restricted three-body problem. Astrophys. Space Sci. 2013; 343: 95–106. doi: 10.1007/s10509-012-1225-0
19. Abouelmagd EI, El-Shaboury SM. Periodic orbits under combined effects of oblateness and radiation in the restricted problem of three bodies. Astrophys. Space Sci. 2012; 341: 331–341. doi: 10.1007/s10509-012-1093-7
20. Abozaid AA, Selim HH, Gadallah KAK, et al. Periodic orbits in the frame work of the restricted three bodies under the asteroids belt effect. Applied Mathematics and Non-linear science. 2015; 1(2): 15–34.
21. Abouelmagd EI, Alhowaity S, Diab Z, et al. On the Periodic Solutions for the Perturbed Spatial Quantized Hill Problem. Mathematics. 2022; 10(4): 614.
22. Ershkov S, Abouelmagd EI, Rachinskaya A. Perturbation of relativistic effect in the dynamics of test particle. Journal of Mathematical Analysis and Applications. 2023; 524(1): 127067.
23. Doshi MJ, Pathak NM, Abouelmagd EI. Periodic orbits of the perturbed relative motion. Advances in Space Research. 2023; 72(6): 2020–2038.
24. Alshaery AA, Abouelmagd EI. Analysis of the spatial quantized three-body problem. Results in Physics. 2020; 17: 103067.
25. Jiang IG, Yeh LC. On the Chermnykh-like problem: I. The mass parameter $\mu = 0.5$. Astrophysics and space science. 2006; 305: 341–348.
26. Jiang IG, Yeh LC. On the Chermnykh-like problem: II. The equilibrium points. Astrophysics and space science. 2006; 306: 189–200.
27. Ansari AA. The circular restricted four- body problem with triaxial primaries and variable infinitesimal mass. Applications and Applied Mathematics: An International Journal. 2018; 13(2): 818–838.
28. Ansari AA, Prasad SN. Generalized Elliptic Restricted Four-Body Problem with Variable Mass. Astron. Lett. 2020; 46: 275–288. doi: 10.1134/S1063773720040015
29. Ansari AA. Kind of Robe's restricted problem with heterogeneous irregular primary of N-layers when outer most layer has viscous fluid. New Astronomy. 2020; 83. doi: 10.1016/j.newast.2020.101496

30. Ansari AA, Abouelmagd EI. Variable mass motion in the Hénon-Heiles system. Modern Physics Letters A. 2021; 36(21).
31. Ansari A, Kellil R, Sahdev S. Numerical exploration of the variable mass test particle on the perturbed cr3b configuration. New Astronomy. 2022; 97(11): 101885.
32. Ansari AA. Kerr-like oblate heterogeneous primaries in PCRFB problem with variable mass infinitesimal body. Modern Physics Letters A. 2024; 39(4).
33. Albidah AB, Ansari AA. Shapes and mass variation effects of the bodies in the generalized elliptic restricted 3-body problem. Astronomy reports. 2023; 67(4): 393–403.
34. Albidah AB, Abdullah. Halo orbits under some perturbations in the cr3b problem. Symmetry. 2023; 15: 418.
35. Bouaziz F, Ansari AA. Perturbed Hill's problem with variable mass. Astron. Nachr. 2021. doi: 10.1002/asna.202113870
36. Bhatnagar KB, Hallan PP. Effect of perturbations in the coriolis and centrifugal forces on the stability of libration points in the restricted problem. Celest. Mech. Dyn. Astron. 1978; 18: 105–112.
37. Kushvah BS. Linear Stability of equilibrium points in the generalized photogravitational Chermnykh's problem. Astrophy. Space Sci. 2008; 318(2): 41–50. doi: 10.1007/s10509-008-9898-0
38. Kumari R, Kushvah BS. Stability regions of equilibrium points in restricted four-body problem with oblateness effects. Astrophy. Space Sci. 2014; 349(2): 693–704.
39. Farrés A, Heiligers J, Miguel N. Road map to L_4 / L_5 with a solar sail. Aerospace Science and Technology. 2019; 95: 105458.
40. Albidah AB, Ansari AA, Kellil R. Interaction of 3-body in the circular restricted problem with variable mass. Astronomy and computing. 2023; 42. doi: 10.1016/j.ascom.2023.100688
41. Abouelmagd EI, Ansari AA. The motion properties of the infinitesimal body in the framework of bicircular Sun perturbed Earth–Moon system. New Astronomy. 2019; 73: 101282.